Relativistic extension of the complex scaling method

A. D. Alhaidari*
Shura Council, Riyadh 11212, Saudi Arabia and Physics Department, King Fahd University of Petroleum and Minerals, Dhahran 31261, Saudi Arabia

(Received 1 March 2007; published 16 April 2007)

We construct a tridiagonal matrix representation for the three-dimensional Dirac-Coulomb Hamiltonian that provides for a simple and straightforward relativistic extension of the complex scaling method. Besides the Coulomb interaction, additional vector, scalar, and pseudoscalar coupling to short-range potentials are also included in the same representation. Using that, we are able to obtain highly accurate values for the relativistic bound states and resonance energies. A simple program code is developed to perform the calculation for a given charge, angular momentum, and potential configuration. The resonance structure in the complex relativistic energy plane is also shown graphically. Illustrative examples are given and we verify that in the nonrelativistic limit one obtains known results. As an additional advantage of this tridiagonal representation, we use it to obtain highly accurate evaluation of the relativistic bound state energies for the Woods-Saxon potential (as a model of nuclear interaction) with the nucleus treated as a solid sphere of uniform charge distribution.

DOI: 10.1103/PhysRevA.75.042707 PACS number(s): 03.65.Nk, 03.65.Pm, 11.80.−m, 03.65.Fd

I. INTRODUCTION

Studying the properties of the resolvent operator (Green's function) associated with the scattering of a projectile by a target is essential to the understanding of both the structure of the target and the interaction of the projectile-target system. For example, bound states and resonance energies are identified with the poles of the Green's function $G(z)=(H-z)^{-1}$ in the complex z-plane, where H is a "complexified" version of the Hamiltonian of the system. Dismissing subtle differences in perturbation theory between resonances and eigenvalues for degenerate states [1], it becomes obvious that the poles of $G(z)$ are the complex eigenvalues of H in the z-plane. Resonance states are boundlike states that are unstable and decay with a rate that increases with the value of the imaginary part of the resonance energy.

In nonrelativistic quantum mechanics, the dynamical behavior of the state of the system in time is contained in the exponential factor e^{-iEt}, where E is the nonrelativistic energy. For stable states, like the bound states, E is real. However, for the decaying resonance states, E is complex with negative imaginary part. Systems with Hermitian Hamiltonians have no states with positive imaginary part for E, which would then blow up in time. Therefore, for systems with a self-adjoint Hamiltonian, energy resonances are located in the lower half of the complex energy plane. Sharp or "shallow" resonances are located below and close to the real energy axis in the complex E-plane. These are more stable. They decay slowly and are easier to obtain than broad or "deep" resonances that are located below, but far from, the real energy axis [2]. Most of the algebraic methods used for the study of resonances are applied directly in the complex energy plane, whereas most of the analytic investigations are done in the complex angular momentum plane [3]. The energy spectrum is the set of poles of the Green's function in the complex energy plane, which consists generally, for one-particle (single channel) Hamiltonian, of three parts.

(1) Discrete set of real points on the negative energy axis corresponding to the bound states.
(2) Discontinuity of the Green's function along the real positive energy line (a branch cut), which corresponds to the continuum scattering states.[1]
(3) Discrete set of points in the lower half of the complex energy plane corresponding to the resonance states.

The basic underlying principle in the various numerical methods used in the study of resonances is that the position of a resonance is stable against variation in all unphysical computational parameters.

Consequently, resonance energies are the subset of the poles of the Green's function $G(E)$, which are located in the lower half of the complex energy plane. One way to uncover these resonances, which are "hidden" below the real line in the E-plane, is to use the complex scaling (also known as complex rotation) method [4]. This method exposes the resonance poles and makes their study easier and manipulation simpler. It has been used successfully in the calculations of resonances in nonrelativistic atomic, chemical, and nuclear physics. In this method, the radial coordinate gets transformed as $r\rightarrow re^{i\theta}$, where θ is a real angular parameter. The effect of this transformation on the pole structure of $G^{\theta}(E)\equiv(H^{\theta}-E)^{-1}$ in the complex E-plane, where H^{θ} is the complex-scaled Hamiltonian, consists of the following:

(1) The discrete bound state spectrum that lies on the negative energy axis remains unchanged.
(2) The branch cut (discontinuity) along the real positive energy axis rotates clockwise by the angle 2θ.
(3) Resonances in the lower half of the complex energy plane located in the sector bound by the new rotated cut line

*Electronic address: haidari@mailaps.org

[1]Generally, this part of the spectrum consists of a set of disconnected energy bands with forbidden energy gaps in between. Each band consists of continuous scattering states with energies bounded within that band.

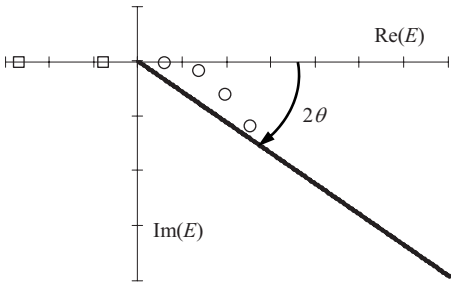

FIG. 1. Full effect of the complex scaling $r \to re^{i\theta}$ on the bound states (squares), continuum (solid line), and resonances (circles) in the nonrelativistic complex energy plane.

and the positive energy axis get exposed and become isolated.

Figure 1 is a graphical representation of this process. However, due to the finite size of the basis set used in the calculation, the matrix representation of the Hamiltonian is finite resulting in a discrete set of eigenvalues (poles of the Green's function). Consequently, the rotated cut line gets replaced by a string of interleaved poles and zeros of the finite Green's function that tries to mimic the cut structure. Additionally, in this finite approximation the 2θ cut line becomes deformed in the neighborhood of resonances due to the effect of localization in the finite L^2 bases in regions that are near to the resonance energies. Figure 2 is a reproduction of Fig. 1 but with a finite basis set. Now, the subset of the eigenvalues that corresponds to the bound states and resonance spectra remain stable against variations in all computational parameters (including θ, as long as these poles are far enough from the cut "line"). For multichannel scattering, on the other hand, there are as many cut lines (branch cuts) as there are channels. Complex scaling causes each cut line to rotate about the corresponding channel's threshold energy point with an angle equal to 2 times the scaling angle of that channel [4].

The basis for the generalization of the complex scaling method to the relativistic problem was first outlined by Weder more than 30 years ago [5]. The mathematical details of this generalization were given later by Šeba [6]. Nonetheless, the implementation of the method on the relativistic problem has been largely ignored in the physics literature for a long time. We are aware of only two recent applications of

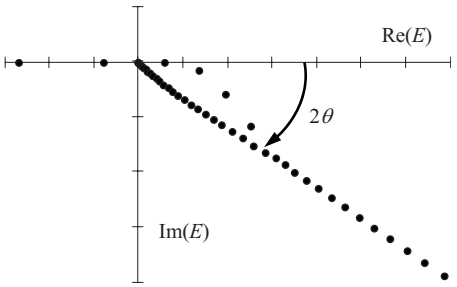

FIG. 2. Showing the same as Fig. 1 but by means of a finite-dimensional basis. The cut line is replaced by a string of dots (eigenvalues of the finite complex rotated Hamiltonian) which is slightly deformed in the neighborhood of resonances.

the method. One is by Ivanov and Ho for computing resonances of hydrogenlike ions in the presence of a uniform electric field [7]. The other is by Pestka *et al.* for obtaining the bound states energies of two-electron atoms within a variational Hylleraas-CI approach [8]. In this work, we present a general and systematic development of an algebraic extension of the complex scaling method to the relativistic problem. The Hamiltonian of the system will be taken to be the three-dimensional Dirac-Coulomb Hamiltonian with an additional coupling to a finite range potential matrix. We assume spherical symmetry and consider three different types of coupling of the Dirac particle to the scattering potential. These are the vector, scalar, and pseudoscalar couplings. In the following section, we construct the spinor basis that results in a tridiagonal matrix representation for the reference Dirac-Coulomb Hamiltonian. The matrix elements of the scattering potential will be calculated in a finite subset of the basis using Gauss quadrature approximation [9]. In Sec. III, we show that this representation makes the application of the complex scaling method to the relativistic problem very simple and straightforward. The resonance structure in the relativistic complex energy plane will be shown graphically. Some potential examples are given and we show that in the nonrelativistic limit we obtain known results. Moreover, we calculate the relativistic bound states energies for the Woods-Saxon potential (as a model for nuclear interaction) in the presence of the Coulomb interaction for a given set of physical parameters and for three different kinds of coupling: vector, scalar, and pseudoscalar. In Sec. IV, we discuss our results and give some ideas about further developments to improve the accuracy of the method. A simple program code (RCS-07.1) was developed, using Mathcad®,[2] to implement the relativistic extension of the complex scaling method and produce all results given in this work. A copy of the code is available upon request from the author.

II. THE TRIDIAGONAL SPINOR REPRESENTATION

In this work, we consider the three-dimensional relativistic scattering problem of spin-$\frac{1}{2}$ charged particle (of mass m) with a massive target. The projectile-target system is described by the time-independent Hamiltonian

$$\mathcal{H} = \mathcal{H}_0 + \mathcal{V} \tag{2.1}$$

The reference Hamiltonian $\mathcal{H}_0$ is taken to be the three-dimensional Dirac Hamiltonian that may include coupling to an exactly solvable 4×4 potential matrix $\mathcal{V}_0$. It is permissible for this "reference potential" to have long-range interaction (e.g., the Coulomb potential). However, the scattering potential matrix $\mathcal{V}$ has finite range such that it is well represented by its matrix elements in a finite square integrable spinor basis. In the units $\hbar = m = e = 1$, the Compton wavelength is $\lambda\!\!\!^{-} = \hbar/mc = 1/c$, which could be written for an electron projectile as $\lambda\!\!\!^{-} = \alpha a_0$, where α is the fine structure constant and a_0 is the Bohr radius. In these units, the reference

[2]Mathcad® is a software package developed by Mathsoft for general-purpose mathematical computations.

Dirac Hamiltonian for the charged spinor with coupling to the electromagnetic four-vector potential $(A_0, c\vec{A})$ reads as follows [10]:

$$\mathcal{H}_0 = \begin{pmatrix} +1+\lambda\!\!\!^{-2}A_0 & -\lambda\!\!\!^{-}\vec{\sigma}\cdot(i\vec{\nabla}+\vec{A}) \\ -\lambda\!\!\!^{-}\vec{\sigma}\cdot(i\vec{\nabla}+\vec{A}) & -1+\lambda\!\!\!^{-2}A_0 \end{pmatrix}, \tag{2.2}$$

where the Hamiltonian is written in units of $mc^2=\lambda\!\!\!^{-2}$ and $\{\vec{\sigma}\}$ are the three 2×2 Hermitian Pauli spin matrices,

$$\sigma_1 = \begin{pmatrix} 0 & 1 \\ 1 & 0 \end{pmatrix}, \quad \sigma_2 = \begin{pmatrix} 0 & -i \\ i & 0 \end{pmatrix}, \quad \sigma_3 = \begin{pmatrix} 1 & 0 \\ 0 & -1 \end{pmatrix}. \tag{2.3}$$

Our choice of atomic units ($\hbar=m=1$) over the conventional relativistic units (where $\hbar=c=1$) is made to allow us to take the nonrelativistic limit, $c\to\infty$ (i.e., $\lambda\!\!\!^{-}\to 0$), in a very simple, intuitive, and straightforward manner which is not possible in the latter units since $c=1$. Additionally, it is easier to compare our results with those in atomic physics since the same system of units is used. Moreover, $mc^2\to\infty$ is not a good measure of the nonrelativistic limit for position-dependent mass systems, which is an interesting problem that is becoming the core of an active field of research. This is because this limit could be violated in regions where the local mass distribution is infinitesimal despite the fact that the system is certainly nonrelativistic.

For the Coulomb interaction, where $A_0=Z/r$ and $\vec{A}=0$, and for spherically symmetric potential $\mathcal{V}(r)$, the angular components separate and the radial reference Dirac Hamiltonian becomes

$$\mathcal{H}_0 = \begin{pmatrix} +1+\lambda\!\!\!^{-2}\dfrac{Z}{r} & \lambda\!\!\!^{-}\left(\dfrac{\kappa}{r}-\dfrac{d}{dr}\right) \\ \lambda\!\!\!^{-}\left(\dfrac{\kappa}{r}+\dfrac{d}{dr}\right) & -1+\lambda\!\!\!^{-2}\dfrac{Z}{r} \end{pmatrix}, \tag{2.4}$$

where Z is the dimensionless electric charge coupling and where length is measured in units of $4\pi\varepsilon_0\hbar^2/me^2$ (for an electron this unit is a_0). The spin-orbit quantum number $\kappa=\pm 1,\pm 2,\ldots$ and it is related to the orbital angular momentum quantum number ℓ by $\kappa=\pm\left(\ell+\frac{1}{2}\right)-\frac{1}{2}$. On the other hand, the radial scattering potential matrix is

$$\mathcal{V}(r) = \lambda\!\!\!^{-}\begin{pmatrix} \lambda\!\!\!^{-}V_+(r) & W(r) \\ W(r) & \lambda\!\!\!^{-}V_-(r) \end{pmatrix}, \tag{2.5}$$

where $V_\pm = V\pm S$. $V(r)$ is the vector potential, $S(r)$ is the scalar potential, and $W(r)$ is the pseudoscalar potential. The reference Dirac-Coulomb problem described by $\mathcal{H}_0$ is exactly solvable. One such solution is obtained (for all energies) as an infinite sum of square integrable functions with expansion coefficients that are orthogonal polynomials in the energy [11]. However, the spinor basis in that solution is energy dependent; a property which is not desirable from a numerical point of view. This is because any calculation in such a basis must be repeated for all energies in the range of interest. Nonetheless, we will use that solution only as a guide to the construction of the spinor basis for the solution space of the present problem. We start by transforming the total radial Hamiltonian using the following 2×2 unitary matrix

$$\mathcal{U}(\varphi) = \exp\left(\frac{i}{2}\varphi\sigma_2\right), \tag{2.6}$$

where φ is a real angular parameter such that $\sin\varphi = \pm\lambda\!\!\!^{-}Z/\kappa$ and where $-\frac{\pi}{2}\leqslant\varphi\leqslant+\frac{\pi}{2}$ depending on the signs of Z and κ. The plus and/or minus sign in $\sin\varphi$ corresponds to the positive and/or negative energy solutions. In what follows, we consider only the positive energy solutions, where $\sin\varphi=\lambda\!\!\!^{-}Z/\kappa$. One can easily show that the negative energy solutions are obtained from the positive energy solutions by exchanging the upper radial spinor component with the lower and applying the following $(\mathcal{CP})$ map

$$\kappa\to-\kappa, \quad Z\to-Z, \quad \text{and } W(r)\to-W(r). \tag{2.7}$$

If we write the transformed Hamiltonian as $H=\mathcal{U}\mathcal{H}\mathcal{U}^{-1}$, then the wave equation reads

$$(H-\varepsilon)\chi(r,\varepsilon)=0, \tag{2.8}$$

where ε is the relativistic energy in units of $mc^2=\lambda\!\!\!^{-2}$. For bound states $|\varepsilon|<1$, whereas for scattering $|\varepsilon|>1$. The transformed reference Hamiltonian becomes

$$H_0 = \mathcal{U}\mathcal{H}_0\mathcal{U}^{-1} = \begin{pmatrix} \dfrac{\gamma}{\kappa}+2\lambda\!\!\!^{-2}\dfrac{Z}{r} & \lambda\!\!\!^{-}\left(-\dfrac{Z}{\kappa}+\dfrac{\gamma}{r}-\dfrac{d}{dr}\right) \\ \lambda\!\!\!^{-}\left(-\dfrac{Z}{\kappa}+\dfrac{\gamma}{r}+\dfrac{d}{dr}\right) & -\dfrac{\gamma}{\kappa} \end{pmatrix}, \tag{2.9}$$

where $\gamma=\kappa\cos\varphi=\kappa\sqrt{1-(\lambda\!\!\!^{-}Z/\kappa)^2}$. On the other hand, we write the transformed scattering potential as

$$U = \mathcal{U}\mathcal{V}\mathcal{U}^{-1} = \lambda\!\!\!^{-}\begin{pmatrix} \lambda\!\!\!^{-}U_+ & U_0 \\ U_0 & \lambda\!\!\!^{-}U_- \end{pmatrix}, \tag{2.10}$$

where

$$U_\pm = \frac{1}{2}(V_+ + V_-) \pm \frac{\gamma}{\kappa}\frac{1}{2}(V_+ - V_-) \pm \frac{Z}{\kappa}W, \tag{2.11a}$$

$$U_0 = \frac{\gamma}{\kappa}W - \lambda\!\!\!^{-2}\frac{Z}{\kappa}\frac{1}{2}(V_+ - V_-). \tag{2.11b}$$

Now, we expand the solution of the wave equation (2.8) as $\chi(r,\varepsilon)=\Sigma_n C_n(\varepsilon)\psi_n(r)$, and write the radial spinor components as

$$\psi_n(r) = \begin{pmatrix} \phi_n^+(r) \\ \phi_n^-(r) \end{pmatrix}. \tag{2.12}$$

Contrary to the basis set used in Ref. [11], these basis elements are taken to be energy independent. The upper radial spinor component reads as follows:

$$\phi_n^+(r) = \begin{cases} a_n^+ x^{\gamma+1}e^{-x/2}L_n^{\nu_+}(x), & \kappa>0, \\ a_n^- x^{-\gamma}e^{-x/2}L_n^{\nu_-}(x), & \kappa<0, \end{cases} \tag{2.13}$$

where $x=\omega r$, $L_n^\nu(x)$ are the associated Laguerre polynomials of order n [12], and the normalization constants are $a_n^\pm$

$=\sqrt{\omega\Gamma(n+1)/\Gamma(n+\nu_\pm+1)}$. The basis parameters ω and $\nu_\pm$ are real such that $\omega>0$, $\nu_\pm>-1$. We are seeking a two-component spinor basis that supports a tridiagonal matrix representation for the reference Hamiltonian H_0. To that end, the lower spinor component should be related to the upper by the "kinetic balance" relation, which is suggested by the reference wave equation $(H_0-\varepsilon)\psi_n=0$. That is,

$$\phi_n^-(r)=\frac{\lambda}{\mu}\left(-\frac{Z}{\kappa}+\frac{\gamma}{r}+\frac{d}{dr}\right)\phi_n^+(r), \tag{2.14}$$

where μ is another real basis parameter. In Ref. [11], exact solvability requirement of the reference (Dirac-Coulomb) problem resulted in the energy-dependent basis by dictating that $\mu=\varepsilon+\gamma/\kappa$. However, here we are interested only in an approximate solution to the full problem that still includes an arbitrary, but short-range, scattering potential $\mathcal{V}(r)$. Therefore, for practical calculations we insist that the parameter μ be energy independent. One can show that the spinor basis defined by Eq. (2.13) and Eq. (2.14) results in a tridiagonal matrix representation for the reference Hamiltonian H_0 only if $\nu_\pm=\pm(2\gamma+1)=2|\gamma|\pm1$. Moreover, taking the limit $\lambda\to0$ of the matrix elements of H_0 gives the correct nonrelativistic matrix elements of the Coulomb Hamiltonian only if $\mu=2$ [13]. Using the differential formula and recursion relations of the Laguerre polynomials [12] in the kinetic balance relation (2.14) with $\mu=2$, we obtain the following:

$$\phi_n^-(r)=\frac{\lambda\omega}{4}a_n^\pm x^{(\nu_\pm-1)/2}e^{-x/2}\left[2\left(\gamma-\frac{Z}{\kappa\omega}(2n+\nu_\pm+1)\right)L_n^{\nu_\pm}(x)-\sigma_-(n+\nu_\pm)L_{n-1}^{\nu_\pm}(x)+\sigma_+(n+1)L_{n+1}^{\nu_\pm}(x)\right], \tag{2.15}$$

corresponding to $\pm\kappa>0$ and where $\sigma_\pm=1\pm(2Z/\kappa\omega)$. Moreover, using the known relations among Laguerre polynomials of different indices, we can finally rewrite the L^2 spinor basis as

$$\psi_n(r)=a_n^+x^\gamma e^{-x/2}\begin{pmatrix}(n+2\gamma+1)L_n^{2\gamma}(x)-(n+1)L_{n+1}^{2\gamma}(x)\\ \frac{\lambda\omega}{4}[\sigma_-(n+2\gamma+1)L_n^{2\gamma}(x)+\sigma_+(n+1)L_{n+1}^{2\gamma}(x)]\end{pmatrix},\quad \kappa>0, \tag{2.16a}$$

$$\psi_n(r)=a_n^-x^{-\gamma}e^{-x/2}\begin{pmatrix}L_n^{-2\gamma}(x)-L_{n-1}^{-2\gamma}(x)\\ -\frac{\lambda\omega}{4}[\sigma_+L_n^{-2\gamma}(x)+\sigma_-L_{n-1}^{-2\gamma}(x)]\end{pmatrix},\quad \kappa<0. \tag{2.16b}$$

Using these and the orthogonality relation of the Laguerre polynomials, we obtain the following tridiagonal basis-overlap matrix (representation of the identity):

$$\langle\psi_n|\psi_m\rangle=\{(2n+\nu_\pm+1)[1+(\lambda\omega/4)^2\rho_+]-\lambda^2\omega Z(\gamma/2\kappa)\}\delta_{nm}-[1-(\lambda\omega/4)^2\rho_-]\{\sqrt{n(n+\nu_\pm)}\,\delta_{n,m+1}+\sqrt{(n+1)(n+\nu_\pm+1)}\,\delta_{n,m-1}\}, \tag{2.17}$$

corresponding to $\pm\kappa>0$ and where $\rho_\pm=1\pm(2Z/\kappa\omega)^2$. Additionally, the matrix elements of the tridiagonal reference Hamiltonian is calculated for $\pm\kappa>0$ as

$$(H_0)_{n,m}=\left\{(2n+\nu_\pm+1)\left[\frac{\gamma}{\kappa}+(\lambda\omega/4)^2\left(4-\frac{\gamma}{\kappa}\right)\rho_+\right]+2\lambda^2\omega Z(1-\gamma/2\kappa)^2\right\}\delta_{nm}-\left[\frac{\gamma}{\kappa}-(\lambda\omega/4)^2\left(4-\frac{\gamma}{\kappa}\right)\rho_-\right]\left[\sqrt{n(n+\nu_\pm)}\,\delta_{n,m+1}+\sqrt{(n+1)(n+\nu_\pm+1)}\,\delta_{n,m-1}\right]. \tag{2.18}$$

Now, since the scattering potential $U(r)$ is short range, then we can assume that it will be well represented by its matrix elements in a finite N-dimensional subset of the basis, $\{\psi_n\}_{n=0}^{N-1}$, for some large enough integer N. Therefore, the matrix elements of the potential $U(r)$, which is still arbitrary, can only be evaluated numerically. If we define the (n,m) sampling element of a real square integrable (but not necessarily differentiable) radial function $F(r)$ by the Laguerre polynomials as the value of the integral

$$F_{nm}^\nu=\sqrt{\frac{\Gamma(n+1)\Gamma(m+1)}{\Gamma(n+\nu+1)\Gamma(m+\nu+1)}}\times\int_0^\infty x^\nu e^{-x}L_n^\nu(x)F(x/\omega)L_m^\nu(x)dx, \tag{2.19}$$

Then, we obtain the following potential matrix elements, for $\pm\kappa>0$:

$$\langle\phi_n^+|U_+|\phi_m^+\rangle=R_{nm}^{\nu_\pm}, \tag{2.20a}$$

$$\langle \phi_n^+|U_0|\phi_m^-\rangle + \langle \phi_n^-|U_0|\phi_m^+\rangle = \pm \frac{\lambda\omega}{2}\Bigg(\sigma_\mp \sqrt{(n_\pm + 2|\gamma|)(m_\pm + 2|\gamma|)} \times (U_0)_{nm}^{2|\gamma|} - \sigma_\pm \sqrt{n_\pm m_\pm}(U_0)_{n\pm1,m\pm1}^{2|\gamma|} + \frac{2Z}{|\kappa|\omega}[\sqrt{n_\pm(m_\pm + 2|\gamma|)}(U_0)_{m,n\pm1}^{2|\gamma|} + \sqrt{m_\pm(n_\pm + 2|\gamma|)}(U_0)_{n,m\pm1}^{2|\gamma|}]\Bigg), \tag{2.20b}$$

$$\langle \phi_n^-|U_-|\phi_m^-\rangle = \left(\frac{\lambda\omega}{4}\right)^2 \{\sigma_\mp^2 \sqrt{(n_\pm + 2|\gamma|)(m_\pm + 2|\gamma|)}(U_-)_{nm}^{2|\gamma|} + \sigma_\pm^2 \sqrt{n_\pm m_\pm}(U_-)_{n\pm1,m\pm1}^{2|\gamma|} + \rho_-[\sqrt{n_\pm(m_\pm + 2|\gamma|)} \times (U_-)_{m,n\pm1}^{2|\gamma|} + \sqrt{m_\pm(n_\pm + 2|\gamma|)}(U_-)_{n,m\pm1}^{2|\gamma|}]\}, \tag{2.20c}$$

where the radial function $R(r)$ in Eq. (2.20a) is defined as $R(r)=(\omega r)U_+(r)$ and $n_\pm = n + \frac{1\pm1}{2}$. Now, for an integer K larger than the chosen size of the basis N, we can use Gauss quadrature [9] to give the following approximate evaluation for the integral (2.19):

$$F_{nm}^\nu \cong \sum_{k=0}^{K-1} \Lambda_{nk}^\nu \Lambda_{mk}^\nu F(\eta_k^\nu/\omega), \tag{2.21}$$

where $\{\Lambda_{nk}^\nu\}_{n=0}^{K-1}$ is the normalized eigenvector associated with the eigenvalue η_k^ν of the $K\times K$ tridiagonal symmetric matrix

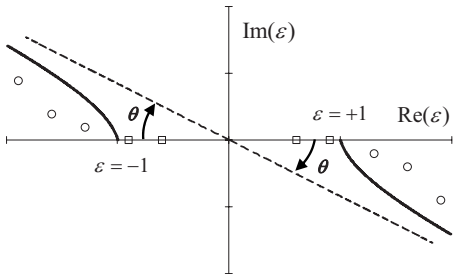

FIG. 3. Effect of the transformation $r \to re^{i\theta}$ on the spectrum of the complex rotated Dirac Hamiltonian. Bound states are shown as squares on the real energy ε axis whereas scattering states are shown as circles. The rotated positive and negative energy continuum are the two solid curves.

TABLE I. A comparison of the relativistic energy of bound states for hydrogenlike ions obtained using the tridiagonal representation in Eq. (2.18) against the exact formula (3.4). The energy variable $\mathcal{E}$ is related to ε by Eq. (3.2) and is measured in units of mc^2. The basis size $N=200$.

Z	j	κ	State	$-\mathcal{E}$ (exact)	$-\mathcal{E}$ (RCS−07.1)
−1	$\frac{1}{2}$	−1	$1S_{1/2}$	0.500000000000	0.50000000142
			$2S_{1/2}$	0.125001664149	0.12500166438
			$3S_{1/2}$	0.055556212996	0.05555621318
		+1	$2P_{1/2}$	0.125001664149	0.12500166439
			$3P_{1/2}$	0.055556212996	0.05555621314
			$4P_{1/2}$	0.031250312026	0.03125031215
	$\frac{3}{2}$	−2	$2P_{3/2}$	0.125000000000	0.12500000002
			$3P_{3/2}$	0.055555719912	0.05555571993
			$4P_{3/2}$	0.031250104007	0.03125010400
		+2	$3D_{3/2}$	0.055555719912	0.05555571992
			$4D_{3/2}$	0.031250104007	0.03125010401
			$5D_{3/2}$	0.020000063902	0.02000006390
−2	$\frac{1}{2}$	−1	$1S_{1/2}$	2.000000000000	2.00000009073
			$2S_{1/2}$	0.500026628513	0.50002664403
			$3S_{1/2}$	0.222232742066	0.22223275140
		+1	$2P_{1/2}$	0.500026628513	0.50002664402
			$3P_{1/2}$	0.222232742066	0.22223275140
			$4P_{1/2}$	0.125004992779	0.12500500038
	$\frac{3}{2}$	−2	$2P_{3/2}$	0.500000000000	0.50000000141
			$3P_{3/2}$	0.222224851984	0.22222485241
			$4P_{3/2}$	0.125001664149	0.12500166439
		+2	$3D_{3/2}$	0.222224851984	0.22222485242
			$4D_{3/2}$	0.125001664149	0.12500166439
			$5D_{3/2}$	0.080001022452	0.08000102263

of the quadrature associated with the Laguerre polynomials $\{L_n^\nu\}$. That is, the matrix whose (n,m) elements are $(2n+\nu+1)\delta_{nm}+\sqrt{n(n+\nu)}\delta_{n,m+1}+\sqrt{(n+1)(n+\nu+1)}\delta_{n,m-1}$ for $n,m=0,1,2,\ldots,K-1$.

In the following section, we show that the representation obtained above is compatible and, in fact, very useful in obtaining the relativistic bound states and resonance energies using the complex scaling method.

III. RELATIVISTIC BOUND STATES AND RESONANCE ENERGIES

Bound states for the one-particle relativistic problem described by the Hamiltonian (2.1) are for energies less than the rest mass. That is the bound states energy spectrum is confined to the real energy interval $\varepsilon\in[-1,+1]$. Moreover, the time dependence of the total spinor wave function for positive (negative) energy, which is given by the exponential factor $e^{-i\varepsilon t}$ ($e^{+i\varepsilon t}$), implies that the imaginary part of resonance energies associated with Hermitian Hamiltonians should be negative (positive). Therefore, resonance energies will be located in the second and fourth quarter of the complex energy plane with $|\mathrm{Re}(\varepsilon)|>1$. Consequently, there will be two energy thresholds for relativistic scattering. These are $\varepsilon=+1$ and $\varepsilon=-1$ for positive and negative energy, respectively. Moreover, there will be two semi-infinite cut lines on the real ε axis corresponding to the continuum scattering states. One for $\varepsilon>+1$ and the other for $\varepsilon<-1$. Thus, the relativistic problem resembles a two-channel nonrelativistic problem (but one with negative energy). Complex scaling causes the two cut lines to rotate clockwise around the origin ($\varepsilon=0$) with an angle θ [5,6,8]. Therefore, these lines will be deformed curving up (down) for energies near $\varepsilon=-1$ ($\varepsilon=+1$). If we parametrize the two cut lines by a real parameter ξ then the effect of the complex scaling transformation $r\to re^{i\theta}$ on the continuous spectrum could be written as the following set of complex numbers [6,8]:

$$\varepsilon(\xi)=\pm\sqrt{\xi^2e^{-2i\theta}+1}. \tag{3.1}$$

For energies close to $\varepsilon=\pm1$ (i.e., in the nonrelativistic limit where ξ is small), these complex scaled curves slope by the angle 2θ as seen from Eq. (3.1). Figure 3 shows the effect of the complex scaling transformation on the complete spectrum of H. Bound states are shown as squares on the real energy axis whereas scattering states are designated by circles. The two rotated cut "lines" are the solid curves. We choose to write all energy values that will be given below in terms of the relativistic energy variable

$$\mathcal{E}(\varepsilon)=(\varepsilon^2-1)/2\lambda^2. \tag{3.2}$$

Therefore, the continuous energy spectrum (the cut lines of the relativistic Green's function) in terms of this complex variable is simply written as $\mathcal{E}(\xi)=\frac{1}{2}(\xi/\lambda)^2e^{-2i\theta}$. This could also be written as $\mathcal{E}=\frac{1}{2}k^2$, where $k=(\xi/\lambda)e^{-i\theta}$ is the complex "relativistic wave number." In the nonrelativistic limit ($\lambda\to0$, $\varepsilon\to1+\lambda^2E$) the energy variable $\mathcal{E}$ will, in fact, be equal to the nonrelativistic energy E.

Now, we show that the matrix representation of the Hamiltonian (2.1) in the spinor basis obtained in the preceding section results in a simple and straightforward scheme for the implementation of the complex scaling method on the relativistic problem. To that end, we write the matrix elements of the total Hamiltonian as

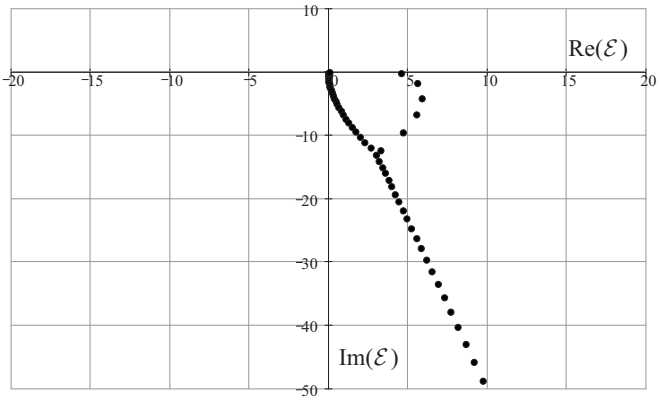

FIG. 4. A snapshot of the video "RCS-07.1" [20] revealing resonance poles in the complex $\mathcal{E}$-plane associated with the potential $V(r)=7.5r^2e^{-r}$, $S(r)=W(r)=0$ and for $Z=1$, $\kappa=-1$. The snapshot is taken at $\theta=0.7$ radians and the basis size $N=100$. Energy is measured in atomic units.

$$\begin{aligned}H_{nm}=\langle\psi_n(x)|H|\psi_m(x)\rangle&=\langle\phi_n^+(x)|\frac{\gamma}{\kappa}+2\lambda^2\omega\frac{Z}{x}|\phi_m^+(x)\rangle\\&-\frac{\gamma}{\kappa}\langle\phi_n^-(x)|\phi_m^-(x)\rangle+\lambda\omega\Big(\langle\phi_n^+(x)|-\frac{Z}{\kappa\omega}+\frac{\gamma}{x}\\&-\frac{d}{dx}|\phi_m^-(x)\rangle+\langle\phi_n^-(x)|-\frac{Z}{\kappa\omega}+\frac{\gamma}{x}+\frac{d}{dx}|\phi_m^+(x)\rangle\Big)\\&+\lambda^2\langle\phi_n^+(x)|U_+(x/\omega)|\phi_m^+(x)\rangle+\lambda^2\langle\phi_n^-(x)|U_-(x/\omega)\\&\times|\phi_m^-(x)\rangle+\lambda[\langle\phi_n^+(x)|U_0(x/\omega)|\phi_m^-(x)\rangle\\&+\langle\phi_n^-(x)|U_0(x/\omega)|\phi_m^+(x)\rangle],\end{aligned} \tag{3.3}$$

where $x=\omega r$. It is, thus, obvious that the effect of the transformation $r\to re^{i\theta}$ on the differential matrix operator $H(r)$ in configuration space is equivalent to the transformation $\omega\to\omega e^{-i\theta}$ of its matrix elements in the spinor representation (2.16). Now, this latter transformation is very easy to implement on the matrix elements (2.17), (2.18), and (2.20) that make up the representation (3.3). One may also note that the $\sqrt{\omega}$ factor in the normalization constant $a_n^\pm$ together with the integration measure dr cooperate to preserve the equivalence between these two transformations by producing the integration measure dx.

We start with a consistency check of the results obtained using the representation given in the preceding section against known exact results. For that purpose we calculate the relativistic energy of the bound states for hydrogenlike ions (where $\lambda=\alpha a_0$ and $\mathcal{V}=0$) and compare that with the exact formula [10]

$$\varepsilon_n=\pm\left[1+\left(\frac{\lambda Z}{n+\tau+1}\right)^2\right]^{-1/2}, \tag{3.4}$$

where $\tau=\left\{\begin{smallmatrix}\gamma,\ \kappa>0\\ -\gamma-1,\ \kappa<0\end{smallmatrix}\right\}$. Throughout our calculation, we use the following strategy. We search for a range of values of the

basis scale parameter ω that give stable results for a given basis size N. We calculate the average result corresponding to several values of ω (preferably, from the middle of the range) keeping only significant digits. Those are the digits that do not change by changing N by, say, 5%. Table I shows a good agreement relative to a basis size $N=200$ and with calculation stability for a range of values of $\omega=1$ to 5 a.u. Nonetheless, built on a general-purpose software package and by an author with limited programming experience, the code used in the calculation is not meant to achieve high precision but to demonstrate the utility and applicability of the extended method. Of course, higher precision could be achieved with better computational routines to find, for example, the generalized eigenvalues and eigenvectors for large tridiagonal matrices. Moreover, since the relativistic energy spectrum (for typical systems) clusters around $\varepsilon = \pm 1$, then to reduce computational errors it is advisable in some cases to calculate the eigenvalues $\varepsilon_n \mp 1$ instead of ε_n, respectively. This is also one of the reasons that we choose to give our results in terms of the energy variable $\mathcal{E}$ instead of ε. Moreover, in the following section we outline further development that should result in a substantial improvement in the accuracy of the calculation by taking into account the full contribution of the reference Dirac-Coulomb Hamiltonian $\mathcal{H}_0$.

To illustrate further the utility and accuracy of the method, we implement it on an atomic model with known nonrelativistic resonance structure. We choose the well-established and frequently used model $V(r)=7.5r^2e^{-r}$ [14–19] and take $S(r)=W(r)=0$ in the potential matrix (2.5). The video "RCS-07.1" [20] shows how the positive energy resonances become exposed as the cut "line" sweeps the lower half of the $\mathcal{E}$-plane, while the angle θ of the complex scaling transformation gradually increases from 0.0 to 0.9 radians. Figure 4 is a snapshot from the same video at $\theta=0.7$ radians. It should be clear that, just like in nonrelativistic scattering, the cut line gets deformed near resonances due to the localization effect. In Table II we compare the nonrelativistic limit of our calculation of the resonance energies associated with this model potential for $\kappa=-1$ ($\ell=0$) against known nonrelativistic results elsewhere. In the calculation, the nonrelativistic limit was achieved by taking $\lambda\!\!\!^{-}/a_0=\alpha/100$. That is, the fine structure constant was effectively reduced by a factor of 100 or, equivalently, the speed of light was ascribed a value 100 times larger. We took a basis size $N=100$ and calculation stability is for a range of

TABLE II. The nonrelativistic limit of our calculation of the resonance energies, $E_r-\frac{i}{2}\Gamma_r$, associated with the model potential $V(r)=7.5r^2e^{-r}$, $S(r)=W(r)=0$, and for $\kappa=-1$ ($\ell=0$) against known nonrelativistic results elsewhere. We took a basis size $N=100$ and the nonrelativistic limit was achieved by scaling down the fine structure constant 100 times.

Z	E_r (a.u.)	Γ_r (a.u.)	Reference
0	3.42639	0.025549	[14]
	3.4257	0.0256	[15]
	3.426	0.0256	[16]
	3.426	0.0258	[17]
	3.426390331	0.025548962	[18]
	3.426390310	0.025548961	[19]
	3.4263903	0.025549	This work
0	4.834806841	2.235753338	[18]
	4.834806841	2.235753338	[19]
	4.8348069	2.2357529	This work
0	5.277279780	6.778106356	[18]
	5.277279864	6.778106591	[19]
	5.2772798	6.7781065	This work
−1	1.7805	9.58×10^{-5}	[17]
	1.780524536	9.5719×10^{-5}	[18]
	1.780524536	9.57194×10^{-5}	[19]
	1.780525	9.59×10^{-5}	This work
−1	4.101494946	1.157254428	[18]
	4.101494946	1.157254428	[19]
	4.101495	1.157254	This work
−1	4.663461099	5.366401539	[18]
	4.663461097	5.366401540	[19]
	4.663461	5.366402	This work

TABLE III. A more comprehensive list of the relativistic energy resonances $\mathcal{E}_r - i\Lambda_r/2$ for the same potential as in Table II, but for several values of Z and κ.

	$\kappa=-1$ $\left(j=\frac{1}{2},\ell=0\right)$		$\kappa=+1$ $\left(j=\frac{1}{2},\ell=1\right)$		$\kappa=-2$ $\left(j=3/2,\ell=1\right)$	
Z	$\mathcal{E}_r$ (a.u.)	Λ_r (a.u.)	$\mathcal{E}_r$ (a.u.)	Λ_r (a.u.)	$\mathcal{E}_r$ (a.u.)	Λ_r (a.u.)
0	2.9465842	23.06811	2.2170	25.8544	2.2170	25.8545
	3.4266874221	0.0255518009	3.80129781	20.19320406	3.801256006	20.19329161
	4.2687950416	17.439000786	4.647141064	0.6506112695	4.6471912798	0.6506993408
	4.8354225415	2.2361196639	4.888143904	14.627813147	4.88811024012	14.627927250
	5.0654945401	11.955326382	5.361234056	4.3953039551	5.36124186636	4.3954504642
	5.2780344286	6.7796704926	5.428512321	9.283011964	5.42849401850	9.2831485326
−1	1.7805455986	0.0000957022	1.92025	24.5794	1.92010	24.5795
	2.592623	21.393386	3.453842379	18.973863298	3.4537211666	18.974083056
	3.8493853286	15.820609152	3.8482370611	0.2752972793	3.8483561762	0.2753948771
	4.1018900840	1.1572503194	4.4767397212	13.480474062	4.47665785037	13.480735107
	4.5617673176	10.415641527	4.7506422650	3.5058292798	4.75066932711	3.5061036576
	4.6640968354	5.3671942790	4.9336803340	8.2353324063	4.93364679163	8.2356163021
+1	3.281076	24.715461	2.503217	27.12133	2.503265	27.12135
	4.5950476252	0.25794882226	4.1363561854	21.403666589	4.136385087	21.403689968
	4.6664918654	19.0235931997	5.2842961861	15.766367118	5.2843094425	15.766398357
	5.54553715604	13.4562601372	5.3726029555	1.1464590251	5.3726223834	1.1465226325
	5.57049606384	3.42295459433	5.9032040396	10.323528755	5.9032078368	10.323575489
	5.86827722644	8.1611145838	5.9418167716	5.2816442304	5.9418208860	5.2817101553

values of $\omega=5-30$ a.u. Here again, we note the good agreement despite the relatively small size of basis (compared to other studies where five-fold to 10-fold larger sizes are typical) and limited programming power. It is worth noting that computational errors increase substantially if one attempts to obtain the nonrelativistic limit by reducing the value of χ too much (for example, by taking $\chi/a_0=10^{-4}\alpha$). Table III gives a more comprehensive list of the relativistic energy resonances ($\mathcal{E}=\mathcal{E}_r-i\Lambda_r/2$) for the same potential as in Table II, but for several values of Z and κ.

As an additional advantage of the tridiagonal representation constructed in the preceding section, we use it in obtaining highly accurate values of the relativistic bound states energies for the Woods-Saxon potential as a model of nuclear interaction. We consider a system consisting of a nucleon and a heavy nucleus of mass number $A \gg 1$ and atomic number Z. In addition to the Coulomb interaction between the nucleon (proton) and the nucleus, we model the nuclear interaction by the Woods-Saxon potential,

TABLE IV. The relativistic S-wave bound state energies (second column) of a neutron in a heavy nucleus where the nuclear interaction is modeled by the Woods-Saxon potential in a vector coupling only and for $V_0=300$ MeV, $R_0=7.0$ fm, and $r_0=0.5$ fm. The nonrelativistic limit (third column) is compared with the exact values (fourth column). We set the basis size $N=100$.

n	$-\mathcal{E}$ (MeV)	$-\mathcal{E}$ $(\chi\to 0)$	$-E$ (exact)
0	248.09714552	294.14089	294.140931652
1	237.05488798	278.11419	278.114215979
2	220.19616375	253.94764	253.947661400
3	198.22742513	222.94965	222.949660882
4	171.69679031	186.18539	186.185386283
5	141.19339459	144.77473	144.774714174
6	107.47368313	100.15691	100.156894346
7	71.63686680	54.63639	54.636364679
8	35.60108366	13.50014	13.500142641
9	4.6544		

$$V_{\mathrm{WS}}(r) = \frac{-V_0}{1+e^{(r-R_0)/r_0}}, \tag{3.5}$$

for a given set of parameters V_0, R_0, and r_0, where $r_0 \ll R_0 \propto A^{1/3}$ [21]. Additionally, for proton scattering, we model the nucleus as a sphere of a uniform charge distribution Ze with charge radius R_c. That is, we write the electrostatic potential as

$$V_C(r) = \lambda^2 \begin{cases} \dfrac{Z}{r}, & r \geqslant R_c, \\ \dfrac{Z}{2R_c}\left[3-\left(\dfrac{r}{R_c}\right)^2\right], & r < R_c. \end{cases} \tag{3.6}$$

Now, there are three different possibilities for the Woods-Saxon potential coupling and combinations thereof. These are the vector, scalar, and pseudoscalar couplings as shown in Eq. (2.5). That is, for a given choice of dimensionless coupling parameters $\{\eta_i\}_{i=V,S,W}$, we take $V(r)=\eta_V V_{\mathrm{WS}}(r)$, $S(r)=\eta_S V_{\mathrm{WS}}(r)$, and $W(r)=\eta_W V_{\mathrm{WS}}(r)$. However, in the nonrelativistic limit the vector and scalar coupling produce the same results, which could also be verified numerically. We start by calculating the bound states energy spectrum for pure vector coupling and for a given choice of physical parameters. We also compare the nonrelativistic limit of our calculation to the exact spectrum, which is known only for $Z=0$ (e.g., for the neutron) and $\kappa=-1$ ($\ell=0$) [22]. Table IV lists these results for $N=100$ showing a good agreement (to seven significant digits) with calculation stability relative to variations in ω in the range from 3 to 30 fm^{-1}. The nonrelativistic limit was achieved by reducing the value of λ 1000 times. Table V gives a more comprehensive list of the relativistic bound state energies for the same potential parameters with $Z=0$ but for different values of κ and for the three types of coupling. In the pseudoscalar coupling case, it is interesting to observe that (1) for $\kappa<0$, there is only one bound state for this configuration, and (2) for $\kappa=+2$, one of the bound state energies is greater then V_0. The last observation could be understood by noting that $W(r)$ belongs to the odd part of the Hamiltonian matrix whereas the energy ε belongs to the even part, consequently its contribution to the energy is of the form W^2 and/or $\pm W'$ which could exceed V_0. This is similar to the known properties of potentials in su-

TABLE V. A more comprehensive list of the relativistic bound state energies ($-\mathcal{E}$, in MeV) for the same potential parameters as in Table IV with $Z=0$ (the neutron) but for different values of angular momentum and for the three types of coupling.

	$\kappa=-1$	$\kappa=+1$	$\kappa=-2$	$\kappa=+2$
Vector coupling	248.09714552	244.07612732	244.05944671	239.11954166
	237.05488798	229.93809634	229.89901505	222.01448951
	220.19616375	210.41012018	210.34426731	199.90042987
	198.22742513	186.06369707	185.96818538	173.25490727
	171.69679031	157.43992621	157.31367275	142.63791463
	141.19339459	125.18794962	125.03227433	108.78351319
	107.47368313	90.19574478	90.01548066	72.75980580
	71.63686680	53.85258438	53.65886815	36.40959785
	35.60108366	18.99802008	18.82018769	4.6367
	4.6544			
Scalar coupling	247.08802455	242.00980035	242.03031833	235.73382171
	233.17051614	224.09763124	224.14624112	213.98597667
	211.78436837	199.22185488	199.30430140	185.74563306
	183.79614007	168.12781475	168.24771957	151.69996208
	149.98319301	131.67265604	131.83052980	112.84625319
	111.38515070	91.14810050	91.33914821	70.83483040
	69.69913447	48.85536144	49.06345008	28.95060786
	28.33017949	10.3822863	10.549754	
Pseudoscalar coupling	24.96939116	209.82627993	11.553984	313.82409795
		106.89104987		209.82714254
		69.11217961		146.52376221
		61.62901889		109.19860821
		36.89889862		93.03720230
		13.7105454		67.10917125
				36.34712447
				6.957939

TABLE VI. Similar to the results in Table V but for the proton where the Coulomb interaction, modeled by the uniform charge sphere in Eq. (3.6), comes into play in addition to the Woods-Saxon potential. We took $V_0=300$ MeV, $R_0=7.0$ fm, $r_0=0.5$ fm, $Z=50$, and $R_c=1.2R_0$.

	$\kappa=-1$	$\kappa=+1$	$\kappa=-2$	$\kappa=+2$
Vector coupling	239.563803170	235.622595549	235.607266173	230.691823560
	228.427148185	221.250580826	221.212660865	213.257784117
	211.338683118	201.429688194	201.364600016	190.794499205
	189.054177508	176.728212555	176.633055235	163.758365131
	162.150372138	147.708047152	147.581800246	132.72573538
	131.24325714	115.04498776	114.88911600	98.4589242
	97.1216445	79.6653740	79.4850046	62.075202
	60.937643	43.036007	42.843025	25.54591
	24.74935	8.29641	8.12416	
Scalar coupling	238.556334402	233.544307761	233.569264591	227.275002469
	224.495382012	215.329897357	215.383392390	205.114952428
	202.804046574	190.075318001	190.163351087	176.431455638
	174.410677933	158.53272069	158.65893774	141.90093621
	140.13449560	121.59641534	121.76120939	102.55848693
	101.0646524	80.6174386	80.8156537	60.132805
	58.983495	38.029052	38.243362	18.14774
	17.55533	0.10888	0.27041	
Pseudoscalar coupling	15.66550	199.916335725	2.5290	305.924565954
		95.557943017		200.016684061
		59.234063046		135.940910601
		50.5104651		98.78339687
		25.936922		83.0367989
		3.0903		56.444298
				25.533513

persymmetric quantum mechanics [23]. Table VI shows similar results to that in Table V but for the proton where the Coulomb interaction (3.6) comes into play in addition to the Woods-Saxon potential. We took $R_c=1.2R_0$ and $Z=50$.

IV. DISCUSSION

In our calculation of bound states and resonance energies, we used a finite N-dimensional basis. However, the matrix representation of the reference Hamiltonian $\mathcal{H}_0$ is fully accounted for as given by Eq. (2.18). It is only the potential matrix $\mathcal{V}$ that must be approximated by its elements in the finite subset of the basis as given by Eqs. (2.20a), (2.20b), and (2.20c). Therefore, the matrix representation of the Hamiltonian, which is available at our disposal, is the following:

$$\mathcal{H}_{nm} \cong \begin{cases} (\mathcal{H}_0)_{nm} + \mathcal{V}_{nm}, & n,m \leqslant N-1, \\ (\mathcal{H}_0)_{nm}, & n,m > N-1. \end{cases} \tag{4.1}$$

Consequently, if one could find the means of handling the infinite tridiagonal tail of this matrix and thus account for the full contribution of $\mathcal{H}_0$ in the calculation, then one should expect to obtain much more accurate results. In fact, such a scheme does exist. The representation (4.1) is the fundamental underlying structure of the J-matrix method [24]. It is an algebraic method of quantum scattering. The method takes into account the full contribution of the reference Hamiltonian analytically. It is in our work plan to combine the relativistic extension of the complex scaling method developed here and the relativistic version of the J-matrix method [13,25] for achieving a substantial improvement on the accuracy for calculating the relativistic energy of bound states and resonances.

ACKNOWLEDGMENTS

The author is grateful to M. S. Abdelmonem for providing some of the reference material cited in Table II. The author is also indebted to him and to H. Bahlouli for suggesting improvements on the original paper. The support provided by the KFUPM library in literature search is highly appreciated. This work is partially supported by KFUPM Grant No. FT-2006/06.

[1] T. Kato, *Perturbation Theory for Linear Operators*, 2nd ed. (Springer, Berlin, 1976).

[2] The volume of publications on resonances in scattering is overwhelming. Books and papers cited in this work and references therein are examples with broad coverage. A good start could be the book by V. I. Kukulin, V. M. Krasnopolsky, and J. Horáček, *Theory of Resonances* (Kluwer, Dordrecht, 1988).

[3] V. De Alfaro and T. Regge, *Potential Scattering* (North-Holland, Amsterdam, 1965); J. R. Taylor, *Scattering Theory* (Wiley, New York, 1972); C. J. Joachain, *Quantum Collision Theory* (North-Holland, Amsterdam, 1975), pp. 260–271; R. G. Newton, *Scattering Theory of Waves and Particles*, 2nd ed. (Springer, New York, 1982), pp. 402–416; A. G. Sitenko, *Scattering Theory* (Springer, Heidelberg, 1991).

[4] J. Aquilar and J. M. Combes, Commun. Math. Phys. **22**, 269 (1971); E. Balslev and J. M. Combes, *ibid.* **22**, 280 (1971); B. Simon, *ibid.* **27**, 1 (1972); Ann. Math. **97**, 247 (1973); C. Cerjan, R. Hedges, C. Holt, W. P. Reinhardt, K. Scheibner, and J. J. Wendoloski, Int. J. Quantum Chem. **14**, 393 (1978); W. P. Reinhardt, Annu. Rev. Phys. Chem. **33**, 223 (1982); B. R. Junker, Adv. At. Mol. Phys. **18**, 208 (1982); A. Maquet, Shih-I Chu, and W. P. Reinhardt, Phys. Rev. A **27**, 2946 (1983); Y. K. Ho, Phys. Rep. **99**, 1 (1983); M. Bylicki, Adv. Quantum Chem. **32**, 207 (1998); N. Moiseyev, Phys. Rep. **302**, 211 (1998).

[5] R. A. Weder, J. Math. Phys. **15**, 20 (1974).

[6] P. Šeba, Lett. Math. Phys. **16**, 51 (1988).

[7] I. A. Ivanov and Y. K. Ho, Phys. Rev. A **69**, 023407 (2004).

[8] G. Pestka, M. Bylicki, and J. Karwowski, J. Phys. B **39**, 2979 (2006).

[9] V. I. Krylov, *Approximate Calculation of Integrals* (Macmillan, New York, 1962); B. Carnahan, H. A. Luther, and J. O. Wilkes, *Applied Numerical Methods* (Wiley, New York, 1969); R. W. Haymaker and L. Schlessinger, in *The Padé Approximation in Theoretical Physics*, edited by G. A. Baker and J. L. Gammel (Academic, New York, 1970).

[10] See, for example, J. D. Bjorken and S. D. Drell, *Relativistic Quantum Mechanics* (McGraw-Hill, New York, 1964); B. Thaller, *The Dirac Equation* (Springer, Berlin, 1992); W. Greiner, *Relativistic Quantum Mechanics: Wave Equations*, 3rd ed. (Springer, Berlin, 2000).

[11] A. D. Alhaidari, Ann. Phys. **312**, 144 (2004).

[12] See, for example, *Handbook of Mathematical Functions*, edited by M. Abramowitz and I. A. Stegun (Dover, New York, 1964); W. Magnus, F. Oberhettinger, and R. P. Soni, *Formulas and Theorems for the Special Functions of Mathematical Physics* (Springer, New York, 1966).

[13] A. D. Alhaidari, H. Bahlouli, A. Al-Hasan, and M. S. Abdelmonem available at http://arxiv.org/abs/physics/0703104 (unpublished).

[14] A. D. Isaacson, C. M. McCurdy, and W. H. Miller, Chem. Phys. **34**, 311 (1978).

[15] C. H. Maier, L. S. Cederbaum, and W. Domcke, J. Phys. B **13**, L119 (1980).

[16] V. A. Mandelshtam, T. R. Ravuri, and H. S. Taylor, Phys. Rev. Lett. **70**, 1932 (1993).

[17] H. A. Yamani and M. S. Abdelmonem, J. Phys. A **28**, 2709 (1995).

[18] S. A. Sofianos and S. A. Rakityansky, J. Phys. A **30**, 3725 (1997).

[19] A. D. Alhaidari, J. Phys. A **37**, 5863 (2004).

[20] See EPAPS Document No. E-PLRAAN-75-146704 for this video that shows how the positive energy resonances become exposed as the cut "line" sweeps the lower half of the $\mathcal{E}$-plane, while the angle θ of the complex scaling transformation gradually increases from 0.0 to 0.9 radians. For more information on EPAPS, see http://www.aip.org/pubservs/epaps.html

[21] For proton scattering where length is measured in fermis (e.g., $\lambda\!\!\!^{-}=0.210\,308\,910\,4$ fm) and energy in MeV, converting the potentials $V_{\pm}(r)$ and $\lambda\!\!\!^{-1}W(r)$ in Eq. (2.5) to the energy units mc^2 (where m is the mass of the proton) is achieved by multiplying them (e.g., the energy parameter V_0) with the conversion factor "0.024 096 606 53." Moreover, in these units the Coulomb potential strength (equivalently, the charge coupling Z) in the reference Hamiltonian (2.4) should be scaled down by the factor "28.819 891 56," which is equal to the unit of length $4\pi\varepsilon_0\hbar^2/me^2$ in fm.

[22] S. Flügge, *Practical Quantum Mechanics* (Springer, Berlin, 1974), p. 165; the nonrelativistic energy spectrum for the Woods-Saxon potential satisfies the equation $\arg\Gamma(2i\alpha) - 2\arg\Gamma(\beta+i\alpha) - \tan^{-1}(\alpha/\beta) + \alpha R_0/r_0 = (n+\frac{1}{2})\pi$, where $\alpha(E) = \frac{r_0}{\hbar}\sqrt{2m(E+V_0)}$, $\beta(E) = \frac{r_0}{\hbar}\sqrt{2mE}$, and $n = 0, \pm 1, \pm 2, \ldots$.

[23] E. Witten, Nucl. Phys. B **185**, 513 (1981); F. Cooper and B. Freedman, Ann. Phys. **146**, 262 (1983); C. V. Sukumar, J. Phys. A **18**, 2917 (1985); A. Arai, J. Math. Phys. **30**, 1164 (1989); F. Cooper, A. Khare, and U. Sukhatme, Phys. Rep. **251**, 267 (1995).

[24] E. J. Heller and H. A. Yamani, Phys. Rev. A **9**, 1201 (1974); **9**, 1209 (1974); H. A. Yamani and L. Fishman, J. Math. Phys. **16**, 410 (1975).

[25] P. Horodecki, Phys. Rev. A **62**, 052716 (2000); A. D. Alhaidari, H. A. Yamani, and M. S. Abdelmonem, *ibid.* **63**, 062708 (2001); A. D. Alhaidari, J. Math. Phys. **43**, 1129 (2002).